

Dynamically equivalent rocking structures

Matthew J. DeJong^{1,*} and Elias G. Dimitrakopoulos²

¹*Department of Engineering, University of Cambridge, Trumpington Street, Cambridge, CB2 1 PZ, UK*

²*The Hong Kong University of Science and Technology, Kowloon Bay, Hong Kong, China*

SUMMARY

Predicting the rocking response of structures to ground motion is important for assessment of existing structures, which may be vulnerable to uplift and overturning, as well as for designs which employ rocking as a means of seismic isolation. However, the majority of studies utilize a single rocking block to characterize rocking motion. In this paper, a methodology is proposed to derive equivalence between the single rocking block and various rocking mechanisms, yielding a set of fundamental rocking parameters. Specific structures that have exact dynamic equivalence with a single rocking block, are first reviewed. Subsequently, approximate equivalence between single and multiple block mechanisms is achieved through local linearization of the relevant equations of motion. The approximation error associated with linearization is quantified for three essential mechanisms, providing a measure of the confidence with which the proposed methodology can be applied. Copyright © 2014 John Wiley & Sons, Ltd.

Received 26 June 2013; Revised 2 January 2014; Accepted 13 January 2014

KEY WORDS: rocking; mechanism; linearization; analytical dynamics

1. INTRODUCTION

Original interest in the rocking response of structures stemmed from the desire to quantify ground accelerations and explain overturning during earthquakes (e.g. [1, 2]), but related research continues to expand. This is partially due to the complex dynamics of very simple rocking systems, for which harmonic steady state modes and overturning envelopes (e.g. [3–6]) are intriguing, even before consideration of sliding and bouncing (e.g. [7, 8]) or multi-block systems (e.g. [9–12]), which rapidly engender untenable complexity for practical applications. Continued research interest also stems from the fact that deterministic methods of reliably predicting rocking response have remained elusive due to poor conditioning of the dynamical system and irregularity of expected ground motions. As a result, the problem has often been tackled from a stochastic perspective (e.g. [2, 13, 14]), generating trends in overturning behavior or probabilistic predictions. Alternatively, overturning has been investigated by considering pulse-type motions, to which rocking structures are particularly vulnerable, and for which deterministic results are achievable (e.g. [15–17]). Quantification of the rocking response to pulse-type motions provides tangible overturning predictions, but the response to ground motions where multiple impulses are influential is both time-dependent and sensitive [14], and again beckons for probabilistic methods.

From a more practical perspective, interest in rocking has expanded because of the peculiar negative stiffness, which is characteristic of rocking motion, and effectively isolates the structure from the full influence of ground motion. While this seismic isolation was exploited by pioneering engineers in the 1970s [18, 19], the use of rocking was limited in practical engineering design, although it is recently

*Correspondence to: Matthew J. DeJong, Department of Engineering, University of Cambridge, Trumpington Street, Cambridge, CB2 1 PZ, UK.

†E-mail: mjd97@eng.cam.ac.uk

gaining momentum [20–22]. Recent applications limit the magnitude of rocking through the use of post-tensioning and energy dissipation, in order to meet compatibility requirements. Thus, the focus of related investigations has shifted from prediction of overturning to prediction of maximum rocking amplitude, or drift, including specification of required post-tensioning stiffness and damping capacity to meet drift limits. While these studies have often preferred computational methods of analysis, they have also inspired analytical investigations that more generally capture the effects of damping on rocking [23].

In this context, there is a need to predict the expected rocking response, whether the concern is possible overturning of nonstructural components, possible collapse of unreinforced masonry structures, or the design of a rocking bridge pier. In practice, rocking structures are assessed using static analysis methods or by using linear elastic response spectra (e.g. [24]), both of which are of limited accuracy [25]. Instead, rocking response spectra could be particularly useful. However, such spectra require rocking structures to be defined by a single set of rocking parameters.

This paper presents a methodology to derive an equivalence between SDOF rocking structures (or mechanisms) and the single rocking block. This would allow rocking response spectra, as well as the vast existing research on the single rocking block, to be more broadly applicable. Exact equivalence between different single block structures is straightforward and is considered first, followed by the consideration of approximate equivalence between single and multiple block structures.

2. REVIEW OF SIMPLE ROCKING STRUCTURES

An archetypal rocking system is the single rocking block subjected to horizontal ground motion (Figure 1). The rocking block is the most studied rocking system, and provides a basis for comparison to other SDOF rocking systems. This section presents the equations of motion for the rocking block and reviews other rocking structures for which a direct equivalence with the rocking block exists. The present study focuses solely on the case of pure rocking behavior: the rotation about alternate bottom corners of the block around the pivot points O and O' (Figure 1).

2.1. The rocking block and the fundamental rocking parameters

Consider a rigid block with semi-diagonal R and slenderness α , as defined in Figure 1, subjected to a horizontal ground motion with acceleration time history $\ddot{u}_g(t)$. If the coefficient of friction is sufficient

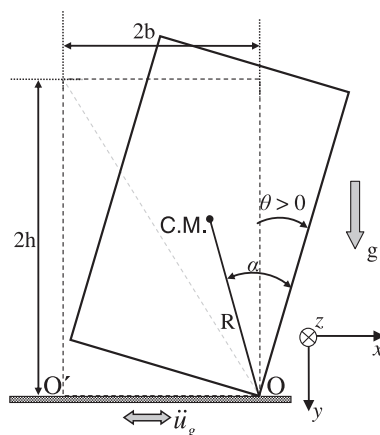


Figure 1. Rocking block geometry.

to prevent sliding, and the block slender enough to avoid bouncing, the block will uplift and commence rocking once the ground acceleration exceeds a minimum magnitude:

$$\lambda = \frac{\ddot{u}_{g,\min}}{g} = \tan \alpha \quad (1)$$

where g is the gravitational acceleration and λ the dimensionless uplift parameter. According to the formulation of Housner [2], the equations of motion during pure rocking are:

$$\begin{aligned} I_O \ddot{\theta}(t) + MgR \sin(+\alpha - \theta(t)) &= -R \cos(+\alpha - \theta) M \ddot{u}_g(t), & \theta(t) > 0 \\ I_O \ddot{\theta}(t) + MgR \sin(-\alpha - \theta(t)) &= -R \cos(-\alpha - \theta) M \ddot{u}_g(t), & \theta(t) < 0 \end{aligned} \quad (2)$$

where I_O is the mass moment of inertia of the block about point O and θ is the rocking rotation (Figure 1). Rearranging Eq. (2) and using the $\text{sgn}()$ function yields

$$\ddot{\theta} = p^2 \left(-\sin[\alpha \text{sgn}(\theta) - \theta] - \frac{\ddot{u}_g}{g} \cos[\alpha \text{sgn}(\theta) - \theta] \right) \quad (3)$$

where p is the rocking frequency parameter, which equals the pendulum frequency of the block when hung about its corner. For a rectangular block (Figure 1), $p = p_{bl} = \sqrt{3g/(4R)}$.

Further, for slender blocks, Eq. (2) can be linearized about the point of unstable equilibrium ($\theta = \theta_{cr} = \alpha$), yielding [2]:

$$\begin{aligned} I_O \ddot{\theta}(t) + MgR(\alpha - \theta(t)) &= -MR \ddot{u}_g(t), & \theta(t) > 0 \\ I_O \ddot{\theta}(t) + MgR(-\alpha - \theta(t)) &= -MR \ddot{u}_g(t), & \theta(t) < 0 \end{aligned} \quad (4)$$

Equation (4) can also be written as:

$$\ddot{\theta} = p^2 \left(-\alpha \text{sgn}(\theta) + \theta - \frac{\ddot{u}_g}{g} \right) \quad (5)$$

Under the assumption of pure rocking, when the block returns to its initial position ($\theta=0$), impact takes place, the pivot point changes, and the rotation switches sign. A simple way to treat impact is with a coefficient of restitution η , which describes the energy dissipated at impact as the ratio of the pre- ($\dot{\theta}^-$) and post- ($\dot{\theta}^+$) impact angular velocities:

$$\dot{\theta}^+ = \eta \dot{\theta}^- \quad (6)$$

The accuracy of this definition of the coefficient of restitution is application and material specific and is beyond the scope of the present paper. Instead, the coefficient of restitution will be treated as an independent parameter in the formulation of the rocking problem, as in [4], allowing implementation of any method of determining its actual value (e.g. [26, 27] and references therein).

Equations (1)–(6) identify four essential parameters that define the response of the rigid rocking block: (i) a frequency parameter p ; (ii) a point of unstable equilibrium θ_{cr} ; (iii) an uplift parameter λ ; and (iv) a damping parameter η . In the case of the rocking block, linearization about the unstable equilibrium position results in a special case where $\lambda_{lin} = \theta_{cr} = \alpha$, so the number of essential parameters is reduced to three. However, this is not generally the case. For other structures, $\lambda \neq \theta_{cr}$ for both the nonlinear and the linearized equations of motion, as discussed in Section 3.

Linearization of the equation of motion about a static configuration, as in Eq. (5), is essential to the proposed approximate equivalence discussed in Section 3. It should be noted that the static configuration where the linearization is applied is important [6, 28], and that the linearized equations of motion become less accurate for non-slender blocks [29]. Further, the magnitude of the error caused by using a linearized formulation is dependent on the magnitude of the rocking response, which is both sensitive and time-dependent. However, trends in linearization error can be observed [29], and indicate

that the size and slenderness of the block, relative to the frequency and amplitude of the ground motion, affect the error. Note that in Section 3 of this study, the focus is instead on quantifying the error associated with the linearization of the mechanisms themselves, independent of the time dependence of the ground motion. Errors for specific ground motion would be less consistent and could be considered separately as in [29].

2.2. Direct equivalence to the single rocking block

Numerous authors have investigated the rocking response of a single rigid block using the formulation of §2.1. Interestingly, the same four rocking parameters ($p, \theta_{cr}, \lambda, \eta$) can also describe the dynamic response (linear or nonlinear) of any symmetric rigid object that rocks about alternating symmetric corners, as well as a select group of more complicated structures. Table I presents three structures that are dynamically equivalent with the rocking block and includes their corresponding rocking parameters. Note that for this table, conservation of angular momentum [2] was used to calculate the damping parameter.

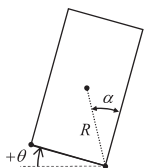
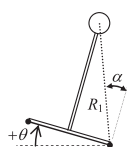
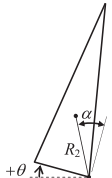
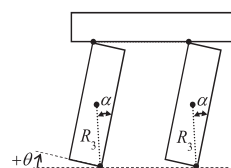
Perhaps the simplest of these structures (Table I) is the point mass on a massless rigid strut with a rigid base, for which the frequency parameter p is readily evident as the natural frequency of a pendulum. The rocking conical shell model (Table I) has been used to evaluate the observed overturning of masonry spires due to horizontal ground motion [30]. A similar model of a cracked spire with a diagonal base (not shown) provided good predictions of experimental results for near-source earthquakes, which contain a dominant primary pulse [31]. In both cases, potential rotation of the conical shell about its vertical axis is ignored.

These equivalences result from different geometries of a single rigid body and, in that sense, are somewhat unsurprising. On the contrary, the symmetric rocking frame (Table I) involves a multiple block mechanism that also exemplifies direct equivalence with the single rocking block [32]. Section 5 demonstrates that the symmetric rocking frame is a special case of a more general class of rocking mechanisms, which are *locally* equivalent to the rocking block. Note that this equivalence is obviously not possible if sliding and bouncing were considered [10, 11], although these effects may be minimal for slender structures subjected to short-duration ground motions.

3. MULTI-BLOCK ROCKING MECHANISMS—PROPOSED METHODOLOGY

A single equation of motion (either Eq. (3) or (5)) describes the response of any of the structures in Table I. Thus, their direct equivalence is somewhat palpable. The present and following sections deal with multiple block mechanisms whose equations of motion are not identical to the pertinent of the rocking block. Instead, an approximate equivalence is sought.

Table I. Rocking structures with direct dynamic equivalence to the single rocking block.

Rocking parameter				
p^2	$\frac{3g}{4R}$	$\frac{g}{R_1}$	$\frac{3g}{4R_2} \frac{16}{3(6 - \sin^2 \alpha)}$	$\frac{3g}{4R_3} \frac{1+2\gamma}{1+3\gamma}$
θ_{cr}			α	
λ			$\tan \alpha$	
η	$\eta_{bl} = 1 - \frac{3}{2} \sin^2 \alpha$	$\eta_{bl} - \frac{1}{2} \sin^2 \alpha$	$\frac{\eta_{bl}}{1 - \frac{1}{6} \sin^2 \alpha}$	$\frac{\eta_{bl} + 3\gamma \cos 2\alpha}{1 + 3\gamma}$

For the frame, $\gamma = m_{beam}/m_{columns}$, where m_{beam} is the mass of the beam and $m_{columns}$ is the combined mass of the columns [32].

In general, the equation of motion for the rocking block, or any rocking mechanism, can be derived using Lagrange's equation:

$$\frac{\partial}{\partial t} \left(\frac{\partial T}{\partial \dot{\phi}} \right) - \frac{\partial T}{\partial \phi} + \frac{\partial V}{\partial \phi} = Q \quad (7)$$

where T is the kinetic energy, V is the potential energy, Q is the generalized force, and ϕ is the generalized coordinate, which describes the rocking motion. For the rocking block, Eq. (7) returns Eq. (2). However, for multiple block mechanisms, Eq. (7) yields an equation of the following form:

$$I_{nl}(\phi)\ddot{\phi} + J_{nl}(\phi)\dot{\phi}^2 - G_{nl}(\phi)g = -B_{nl}(\phi)\ddot{u}_g \quad (8)$$

where I_{nl} , J_{nl} , G_{nl} , and B_{nl} are nonlinear functions of the generalized coordinate, and the point of unstable equilibrium (ϕ_{cr}) is determined from

$$\left. \frac{\partial V}{\partial \phi} \right|_{\phi=\phi_{cr}} = 0 \quad (9)$$

The minimum ground acceleration $\ddot{u}_{g,\min}$ capable of initiating rocking can be determined either from the principle of virtual work, or by substituting $\ddot{\phi} = 0$, $\dot{\phi} = 0$, $\phi = 0$ into Eq. (8):

$$\frac{\ddot{u}_{g,\min}}{g} = \frac{G_{nl}(0)}{B_{nl}(0)} = \lambda \quad (10)$$

There are two essential differences between Eqs. (2) and (8). First, Eq. (8) includes an additional term $J_{nl}(\phi)\dot{\phi}^2$, which describes the centrifugal and Coriolis accelerations. Second, the inertial term $I_{nl}(\phi)$ in Eq. (8) is now a function of the generalized coordinate. These differences prevent straightforward equivalence with the rocking block. Instead, this study utilizes local equivalence with the rocking block at the unstable equilibrium position ($\phi = \phi_{cr}$) to derive an overall approximate equivalence. For small amplitude vibrations about an equilibrium point, Lagrange's equation (7) assumes the linearized form [33]:

$$\left. \frac{\partial^2 T}{\partial \dot{\phi}^2} \right|_{\phi=\phi_{cr}} \ddot{\phi} + \left. \frac{\partial^2 V}{\partial \phi^2} \right|_{\phi=\phi_{cr}} (\phi - \phi_{cr}) = Q|_{\phi=\phi_{cr}} \quad (11)$$

For a multi-block mechanism, Eq. (11) yields

$$I_{eq}\ddot{\phi} - G_{eq}(\phi - \phi_{cr})g = -B_{eq}\ddot{u}_g \quad (12)$$

where G_{eq} , B_{eq} , and I_{eq} are constants that are specific to the kinematics of the unstable equilibrium configuration (Sections 4 and 5):

$$I_{eq} = \left. \frac{\partial^2 T}{\partial \dot{\phi}^2} \right|_{\phi=\phi_{cr}} \quad G_{eq} = - \left. \frac{1}{g} \frac{\partial^2 V}{\partial \phi^2} \right|_{\phi=\phi_{cr}} \quad B_{eq}\ddot{u}_g = -Q|_{\phi=\phi_{cr}} \quad (13)$$

Equation (12) differs from the pertinent equation of the rocking block (4) in that the excitation term is scaled differently than the stiffness term ($B_{eq} \neq G_{eq}$). For this reason, the following transformation of variables is introduced:

$$\theta(t) = \frac{\phi(t)}{\kappa} \quad (14)$$

where θ represents the rotation of the equivalent single block, while ϕ represents the rocking rotation of the multi-block mechanism, and further

$$\kappa = \kappa_1 = \frac{B_{eq}}{G_{eq}} \quad (15)$$

With the help of the transformation (14), the equation of motion (12) assumes the form:

$$\ddot{\theta} = p_{eq}^2 \left(-\theta_{cr} + \theta - \frac{\ddot{u}_g}{g} \right) \quad (16)$$

which is now directly equivalent with (5), and for which

$$p_{eq} = \sqrt{\frac{gG_{eq}}{I_{eq}}} \quad ; \quad \theta_{cr} = \frac{\phi_{cr}}{\kappa} \quad (17)$$

As for the rocking block in Section 2, the uplift acceleration is affected by the linearization, and for Eq. (12), it becomes

$$\frac{\ddot{u}_{g,\min}}{g} = \frac{G_{eq}}{B_{eq}} \phi_{cr} = \lambda_{lin} \quad (18)$$

Hence, the scaling parameter (15) can be written as

$$\kappa_1 = \frac{\phi_{cr}}{\lambda_{lin}} \quad (19)$$

In general, λ_{lin} is an approximation of the exact value λ from Eq. (10). For the rocking block, the difference between these two values increases as the block becomes less slender. It is not always evident whether more complicated rocking structures (Sections 4 and 5) are effectively slender or stocky, but the ratio between λ_{lin} and λ provides a useful measure to quantify effective slenderness. For non-slender structures, an alternate definition of the scaling parameter is desirable:

$$\kappa = \kappa_2 = \frac{\phi_{cr}}{\lambda} \quad (20)$$

Note that the definition of Eq. (20) meets the uplift boundary conditions of the nonlinear system, whereas definition (19) does not. Thus, use of Eqs. (17) and (20) together result in an equivalent block approximation where linearization about the rest position is used to determine κ_2 , while linearization about the point of unstable equilibrium is used to determine p_{eq} . Sections 4 and 5 investigate the effects of these approximations.

The methodology proposed earlier hinges on a local approximation of the nonlinear equations of motion around the unstable equilibrium position. In practice, civil engineering structures experience relatively small rotations, so the study of critical configurations may be adequate. Further, the error associated with ground motion prediction is large, so the error associated with linearization may be acceptable. Physically, and in particular dynamically, multiple block rocking mechanisms are similar to the single rocking block when (i) they can be modeled as SDOF systems; (ii) the different kinematics are locally similar; and (iii) the self-weight restoring mechanism generates the characteristic negative stiffness of rocking behavior. These conditions yield structures that can be described by three fundamental mechanical mechanisms: the pendulum, the slider-crank, and the four-bar linkage. The previous section considered the pendulum or single block mechanism. The following sections consider the slider-crank (two-block) mechanism and the four-bar linkage (three-block mechanism).

4. TWO-BLOCK MECHANISMS—THE ROCKING MASONRY WALL

Consider the slider-crank mechanism shown in Figure 2. Several studies (e.g. [34–36]) adopt this fundamental mechanical configuration, or variations of it, to study the out-of-plane behavior of masonry walls. Variations of this mechanism, which consider additional loads or mass from adjacent structure, could be considered in a similar fashion, but only the unloaded wall is considered here. Using the rotation ϕ (Figure 2) as the generalized coordinate, the nonlinear equation of motion of this rocking structure (direction shown) is

$$\left(\frac{I_O}{2mgR} + \frac{2R}{g} \sin^2(\alpha - \phi)\right) \ddot{\phi} - \frac{R}{g} \sin 2(\alpha - \phi) \dot{\phi}^2 + \sin(\alpha - \phi) = -\frac{1}{2} \frac{\ddot{u}_g}{g} \cos(\alpha - \phi) \quad (21)$$

where I_O is the mass moment inertia of one block about its corner. Note that Eq. (21) is of the same form as Eq. (8). Linearization of Eq. (21) about the unstable equilibrium position ($\phi_{cr} = \alpha$) yields

$$\frac{2R}{3g} \ddot{\phi} = \phi - \phi_{cr} - \frac{1}{2} \frac{\ddot{u}_g}{g} \quad (22)$$

According to Eq. (15), $\kappa_1 = 1/2$, and the transformation of variables in Eq. (14) yields

$$\ddot{\theta} = p_{wall}^2 \left(\theta - \theta_{cr} - \frac{\ddot{u}_g}{g} \right) \quad (23)$$

where $p_{wall} = \sqrt{2}p_{bl} = \sqrt{3g/2R}$ and $\theta_{cr} = 2\alpha$ through the use of Eq. (17), and $\theta(t) = 2\phi(t)$ according to Eq. (14).

The error associated with linearization arises from the approximation of the frequency parameter p and the scaling parameter κ , both of which are constant in the linearized formulation but vary with the rocking rotation in the nonlinear formulation. The frequency parameter p essentially defines the period of free rocking as a function of the rotation angle. If no ground motion occurs, then κ has no effect on the results. To evaluate the error associated with the approximation of p alone (independent of κ), the error in free rocking period ($T_{r,blockeq}/T_{r,wall}$) is plotted as a function of rotation angle (ϕ/ϕ_{cr}) and slenderness (α) in Figure 3 (top left). The free rocking period of the rocking wall $T_{r,wall}$ was calculated numerically using Eq. (21), while the free rocking period of the equivalent block [2] is:

$$T_{r,blockeq} = \frac{4}{p_{eq}} \cosh^{-1} \left(\frac{1}{1 - \theta/\theta_{cr}} \right) \quad (24)$$

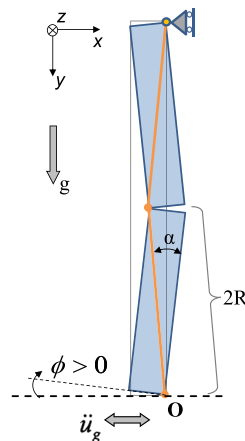


Figure 2. Rocking wall geometry.

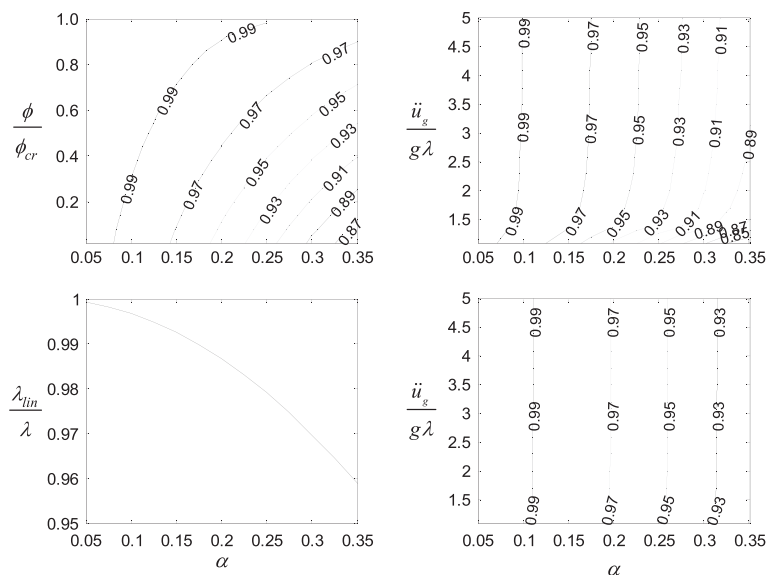


Figure 3. Evaluation of the equivalent block approximation of the masonry wall: free rocking period error ($T_{r,blockeq}/T_{r,wall}$) (top left), uplift parameter error (bottom left), and overturning time error ($t_{over,blockeq}/t_{over,wall}$) using κ_1 (top right) and κ_2 (bottom right).

To evaluate the error associated with κ , a forced response must be considered. A constant horizontal ground acceleration of infinite duration was specified, and the time required ($t_{over,wall}$) for the wall to reach the point of overturning instability ($\phi = \phi_{cr}$) was determined numerically using Eq. (21). The overturning time for the equivalent block described by Eqs. (16) and (19) is [2]:

$$t_{over,blockeq} = \frac{1}{p_{eq}} \cosh^{-1} \left(\frac{1}{\frac{\ddot{u}_g}{g\lambda} \frac{\lambda}{\lambda_{in}} - 1} + 1 \right) \tag{25}$$

Figure 3 (top right) shows the error in overturning time ($t_{over,blockeq}/t_{over,wall}$) as a function of the magnitude of the ground acceleration normalized by the wall uplift acceleration ($\ddot{u}_g/g\lambda$) and the slenderness (α). Note that the absolute overturning time is not of interest, but the ratio of overturning times provides a simple and consistent measure of the magnitude of the error in the forced response through the entire range of motion of the structure.

The results indicate a relatively small magnitude of error for slender walls ($\alpha < 0.2$). The error in free rocking period is least near the point of unstable equilibrium, the point about which the equation of motion is linearized. While these errors are not ideal, they may be acceptable considering the accuracy of earthquake prediction.

For the wall under consideration, $\kappa_1 = 1/2$, while $\kappa_2 = \alpha/2 \tan \alpha$. The difference between these scaling parameters arises from the difference between λ and λ_{in} , which is shown in Figure 3 (bottom left). Using κ_2 instead of κ_1 , the overturning time error is shown in Figure 3 (bottom right). The largest difference in overturning time errors is seen for values of $\ddot{u}_g/g\lambda$ near unity, where the response is obviously sensitive to the assumed uplift acceleration. Regardless, for this structure, the selection of the scaling parameter has a relatively small effect on both the uplift accelerations and the overturning time errors, so use of either κ_1 or κ_2 may be appropriate. However, this is not generally the case.

5. THREE-BLOCK MECHANISMS

This section examines two more complicated rocking structures: the asymmetric rocking frame and the rocking arch. Under specific assumptions, both structures exhibit a three-block rocking mechanism. For

the asymmetric rocking frame, the pivot points are predefined but the rocking mechanism differs depending on the sign of the rocking rotation. The rocking arch, on the other hand, displays a symmetric rocking configuration with respect to the sign of the rocking rotations, but the pivot points are not known a priori.

5.1. The asymmetric rocking frame

A more general case of the two-column rocking frame in Table I is an asymmetric rocking frame (Figure 4). During rocking, the two piers do not exhibit the same rotation, which causes the connecting beam to both translate and rotate. As a result, the kinematics becomes more complicated and the mechanism bears more resemblance to the rocking arch (Figure 9) than to the symmetric rocking frame. Defining the properties of an equivalent rocking block becomes a more tedious and challenging task.

Figure 4 illustrates the assumed three-block mechanisms for clockwise (positive) and anticlockwise (negative) rotations. The pivot points are A, B, C, and D for positive rotations (Figure 4 left) and A', B', C', and D' for negative rotations (Figure 4 right). In both cases, it is assumed that no sliding occurs. Note that the two mechanisms are not identical (Figure 4). For positive rotations, the distance $r_{BC,p}$ (measured from B to the center of mass G_{BC}) is larger, and the angle $\psi_{BC,p}$ is smaller than the corresponding distance $r_{BC,n}$ and angle $\psi_{BC,n}$ for negative rotations. For this reason, depending on the sign of the rocking rotation, the following substitutions must be made in Eqs. (27)–(38):

$$\begin{aligned}
 I_{BC} &= I_{BC,p}, \quad r_{BC} = r_{BC,p}, \quad \psi_{BC} = \psi_{BC,p}, \quad \text{for } \phi = \phi_{0p} - \phi > 0 \\
 I_{BC} &= I_{BC,n}, \quad r_{BC} = r_{BC,n}, \quad \psi_{BC} = \psi_{BC,n}, \quad \text{for } \phi = \phi_{0n} - \phi < 0
 \end{aligned}
 \tag{26}$$

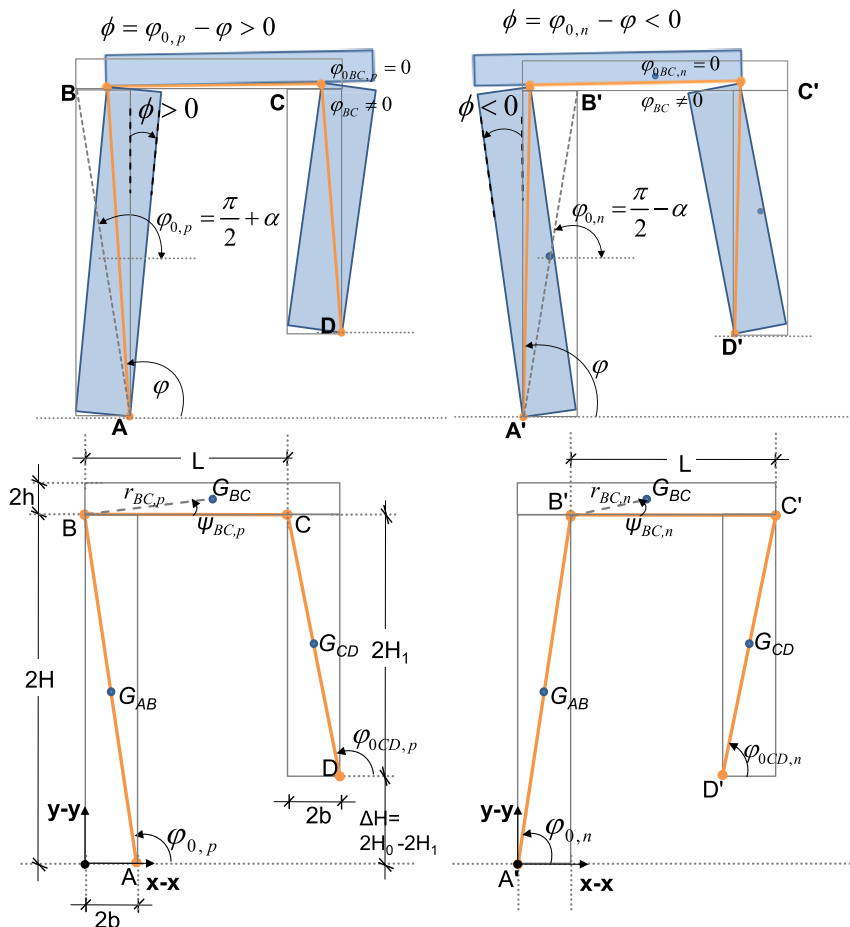


Figure 4. Geometry of the asymmetric rocking frame.

where subscript p corresponds to positive rotations (Figure 4, left) and subscript n to negative rotations (Figure 4, right).

5.1.1. Kinematic analysis. The rich kinematics of the three-block mechanism (i.e. four-bar linkage) of Figure 4 has been examined extensively in the literature of machines and mechanisms. The following analysis is confined to the needs of the present study.

The instantaneous configuration of the three-block mechanism can be captured with a single generalized coordinate, which is selected as the angle φ of segment AB with respect to the positive x -axis. The rocking amplitude is measured as the rotation with respect to the initial position ($\phi = \varphi_0 - \varphi$) in both directions. The orientation of bars BC and CD, with respect to the positive x -axis can be written as a function of the generalized coordinate and known geometry:

$$\begin{aligned}\varphi_{BC}(\varphi) &= \arctan \left[\frac{-R_0 \sin \varphi + r_0 \sin \varphi_{AD} + R_1 \sin \varphi_{CD}(\varphi)}{-R_0 \cos \varphi + r_0 \cos \varphi_{AD} + R_1 \cos \varphi_{CD}(\varphi)} \right] \\ \varphi_{CD}(\varphi) &= \arctan \left(\frac{R_0 \sin \varphi - r_0 \sin \varphi_{AD}}{R_0 \cos \varphi - r_0 \cos \varphi_{AD}} \right) - \arccos \left[\frac{BD^2(\varphi) + 4R_1^2 - L^2}{4R_1 \cdot BD(\varphi)} \right]\end{aligned}\quad (27)$$

where R_0 , R_1 , and r_0 are the half-lengths of blocks AB, BC, and AD, respectively (Figure 4). The angular velocities are then derived from the pertinent rotations by differentiating with respect to time:

$$\dot{\varphi}_{BC}(\varphi, \dot{\varphi}) = \frac{\partial \varphi_{BC}}{\partial \varphi} \dot{\varphi} = f_{BC}(\varphi) \cdot \dot{\varphi}, \quad \dot{\varphi}_{CD}(\varphi, \dot{\varphi}) = \frac{\partial \varphi_{CD}}{\partial \varphi} \dot{\varphi} = f_{CD}(\varphi) \cdot \dot{\varphi}\quad (28)$$

where $\dot{\varphi}$ is the angular velocity of member AB, and the functions f_{BC} and f_{CD} express the rate of change of the rotations φ_{BC} and φ_{CD} with respect to φ . Therefore:

$$f'_{BC}(\varphi) = \frac{\partial^2 \varphi_{BC}}{\partial \varphi^2}, \quad f'_{CD}(\varphi) = \frac{\partial^2 \varphi_{CD}}{\partial \varphi^2}\quad (29)$$

5.1.2. Equation of motion. The potential energy of the three-block mechanism can be expressed as

$$V = g[(m_{AB} + 2m_{BC})R_0 \sin \varphi + m_{BC}r_{BC} \sin(\varphi_{BC} + \psi_{BC}) + m_{CD}(2H - 2H_1 + R_1 \sin \varphi_{CD})]\quad (30)$$

where m_{AB} , m_{BC} , and m_{CD} are the masses of blocks AB, BC, and CD, respectively. The kinetic energy can be expressed as

$$\begin{aligned}T &= \frac{1}{2}I_{AB}\dot{\varphi}^2 + \frac{1}{2}I_{BC}(f_{BC}(\varphi) \cdot \dot{\varphi})^2 + \frac{1}{2}I_{CD}(f_{CD}(\varphi) \cdot \dot{\varphi})^2 \\ &\quad + \frac{1}{2}m_{BC} \left[(2R_0)^2 + 4R_0r_{BC} \cos(\varphi - \varphi_{BC} - \psi_{BC})f_{BC}(\varphi) \right] \dot{\varphi}^2\end{aligned}\quad (31)$$

where I_{AB} is the mass moment of inertia of AB with respect to the pivot point A, and I_{BC} and I_{CD} are the equivalent quantities for members BC and CD.

The equation of motion is derived from Lagrange’s equation (7) and takes the form of Eq. (8), where

$$\begin{aligned}
 I_{nl}(\varphi) &= \left\{ \begin{aligned} &I_{AB} + I_{BC}(f_{BC}(\varphi))^2 + I_{CD}(f_{CD}(\varphi))^2 + \\ &m_{BC}4R_0[R_0 + r_{BC} \cos(\varphi - \varphi_{BC} - \psi_{BC})f_{BC}(\varphi)] \end{aligned} \right\} \\
 J_{nl}(\varphi) &= - \left\{ \begin{aligned} &I_{BC}f_{BC}(\varphi)f'_{BC}(\varphi) + I_{CD}f_{CD}(\varphi)f'_{CD}(\varphi) + 2m_{BC}R_0r_{BC}[\cos(\varphi - \varphi_{BC} - \psi_{BC})f'_{BC}(\varphi)] \\ &-\sin(\varphi - \varphi_{BC} - \psi_{BC})(1 - f_{BC}(\varphi))f_{BC}(\varphi) \end{aligned} \right\} \\
 G_{nl}(\varphi) &= - \{ (m_{AB} + 2m_{BC})R_0 \cos \varphi + m_{BC}r_{BC} \cos(\varphi_{BC} + \psi_{BC})f_{BC}(\varphi) + m_{CD}R_1 \cos \varphi_{CD}f_{CD}(\varphi) \} \\
 B_{nl}(\varphi) &= \left\{ \begin{aligned} &m_{AB}R_0 \sin \varphi + m_{CD}R_1 \sin[\varphi_{CD}(\varphi)]f_{CD}(\varphi) \\ &+ m_{BC}[2R_0 \sin \varphi + r_{BC} \sin[\varphi_{BC}(\varphi) + \psi_{BC}]f_{BC}(\varphi)] \end{aligned} \right\}
 \end{aligned} \tag{32}$$

5.1.3. *Essential rocking parameters.* The minimum ground acceleration required to initiate rocking assumes different values for positive and negative rocking rotations. Applying Eq. (10) for the two rocking mechanisms in Figure 4 yields

$$\lambda = \frac{\ddot{u}_{g,\min}}{g} = \frac{b}{H} \frac{m_{AB} + \left[1 \pm \frac{H}{H_1} - \frac{2b}{L} \left(1 - \frac{H}{H_1} \right) \right] m_{BC} + \frac{H}{H_1} m_{CD}}{m_{AB} + 2 \left[\frac{bh}{LH} \left(1 - \frac{H}{H_1} \right) + 1 \right] m_{BC} + m_{CD}} \tag{33}$$

where the positive sign corresponds to positive rotations, while the negative sign to negative rotations. The critical rotation can be found using Eq. (9), which takes the following form:

$$\begin{aligned}
 &\left(\frac{m_{AB}}{m_{BC}} + 2 \right) \sin[\varphi_{CD}(\varphi_{cr}) - \varphi_{BC}(\varphi_{cr})] \cos \varphi_{cr} + \frac{m_{CD}}{m_{BC}} \sin[\varphi_{cr} - \varphi_{BC}(\varphi_{cr})] \cos \varphi_{CD}(\varphi_{cr}) \\
 &+ \left[\cos \varphi_{BC}(\varphi_{cr}) \left(1 \pm \frac{2b}{L} \right) - \frac{2h}{L} \sin \varphi_{BC}(\varphi_{cr}) \right] \sin[\varphi_{cr} - \varphi_{CD}(\varphi_{cr})] = 0
 \end{aligned} \tag{34}$$

where again the positive sign corresponds to positive rotations, while the negative sign to negative rotations. The critical rotation can then be determined numerically.

5.1.4. *Symmetric frame.* Equations (27)–(34) also describe the behavior of the symmetric rocking frame (Table I), for which $\varphi_{BC}=0$, $\varphi_{CD}=\theta$, $I_0=I_{AB}=I_{CD}$, $R=R_0=R_1$, and $m=m_{AB}=m_{CD}$. In particular, the equation of motion (8) simplifies to

$$(I_0 + 2m_{BC}R^2)\ddot{\varphi} = -(m + m_{BC})R(g \cos \varphi - \ddot{u}_g \sin \varphi) \tag{35}$$

Using Eq. (33), the uplift parameter becomes

$$\lambda = \frac{\ddot{u}_{g,\min}}{g} = \frac{b}{H} \frac{m_{AB} + 2m_{BC} + m_{CD}}{m_{AB} + 2m_{BC} + m_{CD}} = \tan \alpha \tag{36}$$

Using Eq. (34), the critical rotation is simply

$$\varphi_{cr} = \frac{\pi}{2} \Rightarrow \phi_{cr} = \varphi_0 - \varphi_{cr} = \left(\frac{\pi}{2} + \alpha \right) - \frac{\pi}{2} \Rightarrow \phi_{cr} = \alpha \tag{37}$$

Hence, Eqs. (35)–(37) verify the direct equivalence between the symmetric rocking frame and a rocking block, as previously identified [32]. However, because of the different kinematics of the asymmetric frame, this direct equivalence is lost.

5.1.5. Linearized equation of motion. Using the approach outlined in Section 3, the equation of motion can be linearized about the point of (unstable) equilibrium using Eq. (11), written in the form of Eq. (12), in which

$$\begin{aligned}
 I_{eq} &= \left\{ \begin{aligned} &I_{AB} + I_{BC}f_{BC}(\varphi_{cr})^2 + I_{CD}f_{CD}(\varphi_{cr})^2 + \\ &m_{BC}4R_0[R_0 + r_{BC}\cos(\varphi_{cr} - \varphi_{BC}(\varphi_{cr}) - \psi_{BC})f_{BC}(\varphi_{cr})] \end{aligned} \right\} \\
 G_{eq} &= - \left\{ \begin{aligned} &m_{BC}r_{BC}[\cos(\varphi_{BC}(\varphi_{cr}) + \psi_{BC})f'_{BC}(\varphi_{cr}) - \sin(\varphi_{BC}(\varphi_{cr}) + \psi_{BC})(f_{BC}(\varphi_{cr}))^2] \\ &+ m_{CD}R_1[\cos(\varphi_{CD}(\varphi_{cr}))f'_{CD}(\varphi_{cr}) - \sin(\varphi_{CD}(\varphi_{cr}))(f_{CD}(\varphi_{cr}))^2] - (m_{AB} + 2m_{BC})R_0\sin\varphi_{cr} \end{aligned} \right\} \\
 B_{eq} &= \left\{ \begin{aligned} &m_{AB}R_0\sin\varphi_{cr} + m_{CD}R_1\sin(\varphi_{CD}(\varphi_{cr}))f_{CD}(\varphi_{cr}) \\ &+ m_{BC}[2R_0\sin\varphi_{cr} + r_{BC}\sin(\varphi_{BC}(\varphi_{cr}) + \psi_{BC})f_{BC}(\varphi_{cr})] \end{aligned} \right\}
 \end{aligned} \tag{38}$$

As a direct consequence of its lack of symmetry, the rocking frame displays a behavior similar to a nonsymmetric rocking block (e.g. [37–39]); its dynamic (rocking) properties differ with the direction of rocking motion. Using the substitutions of Eq. (26), Eq. (38) yields the constants that describe the rocking mechanisms for clockwise (positive) and anticlockwise (negative) rotations.

Figure 5 presents the dynamic parameters of the equivalent block for a large range of geometries of the asymmetric rocking frame. The left column contains results for a range of geometries with a relatively square aspect ratio and a relatively slender cross beam, resulting in less error associated with the linearized uplift parameter. On the other hand, the right column contains results for frames with a relatively extreme aspect ratio, and a very thick cross beam, so as to purposely induce a larger error associated with the linearized uplift parameter. The subscripts p and n specify the rocking direction. For example, $\phi_{cr,p}/\alpha = (\varphi_{cr} - \varphi_{0p})/\tan^{-1}(b/H)$ denotes the critical rocking rotation in the positive (clockwise) direction scaled over the slenderness of the left column. For $H_1/H = 1$, the frame is symmetric, while as H_1/H becomes larger the rocking properties in the two directions differ more, reflecting the asymmetry of the structure.

Figures 6–8 present the error associated with the proposed methodology similarly to the rocking wall (Section 4). In particular, Figure 6 presents the error associated with the approximation of p alone (independent of κ), as a function of the rotation angle, the rocking direction, and the geometry of the frame. Figures 7 and 8 estimate the error associated with κ_1 and κ_2 , respectively, considering again the time required for the frame to reach the point of overturning under a constant horizontal ground acceleration of infinite duration ($t_{over,frame}$). As a general rule, for slightly asymmetric frames, the errors introduced by the proposed linearized approach are acceptable. Frames with higher asymmetry are not considered because the assumption of pure rocking might be less reasonable.

5.2. The rocking arch

The rocking arch can also be described as a three-block mechanism. Following the formulation of Oppenheim [40], the arch is assumed to form a mechanism (Figure 9, left) when subjected to horizontal ground motion. When the arch returns to its initial position, impact occurs, and the mechanism is assumed to reflect about the vertical line of symmetry (Figure 9, right). Thus, the structure is in some ways similar to the rocking wall, as the positive and negative rocking mechanisms are the same. However, the structure also resembles the asymmetric rocking frame, as it is comprised of a three-block mechanism, for which Coriolis and centrifugal acceleration terms are present in the equations of motion.

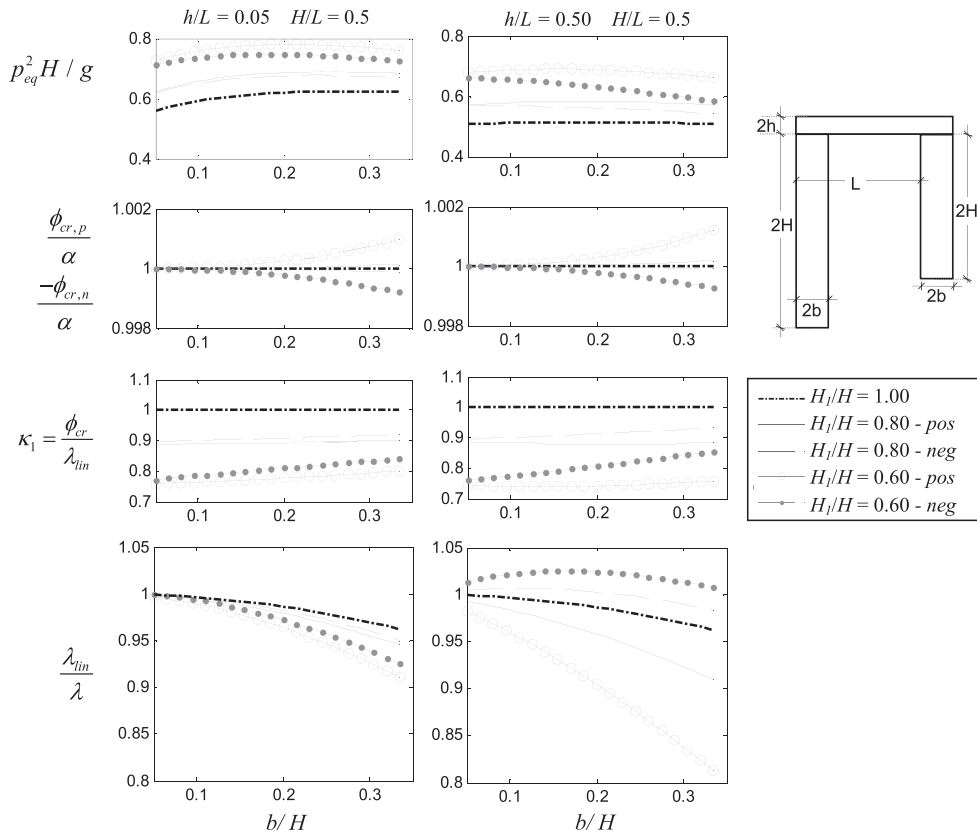


Figure 5. The dynamic properties of an equivalent rocking block for different geometries and rocking directions of the asymmetric frame.

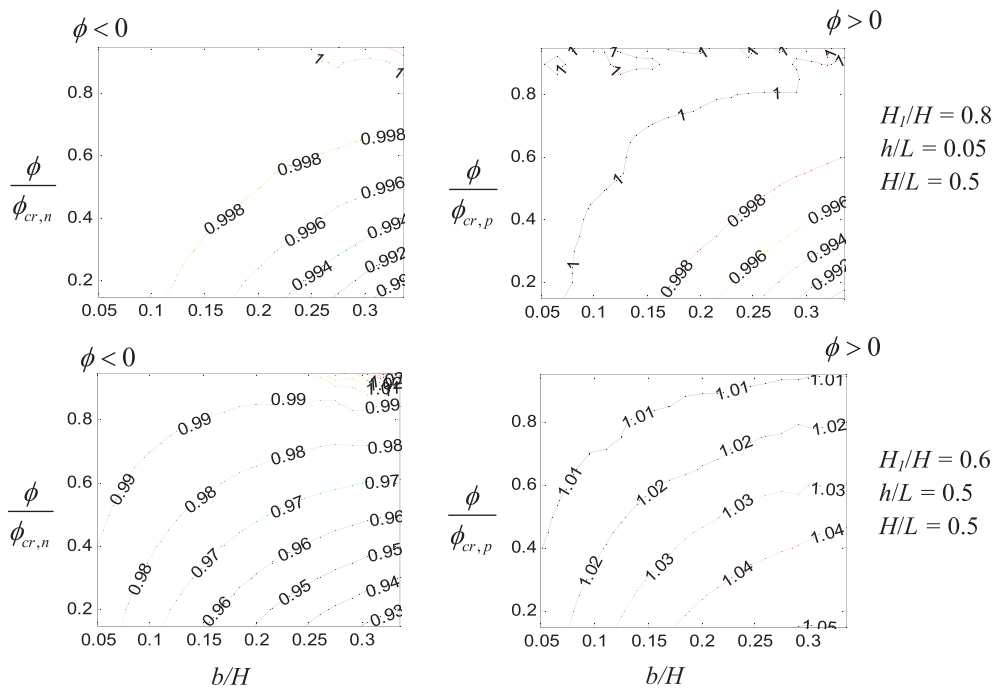


Figure 6. Evaluation of the equivalent block approximation of the asymmetric frame: free rocking period error ($T_{r,blockeq}/T_{r,frame}$) for different rocking directions and frame geometries

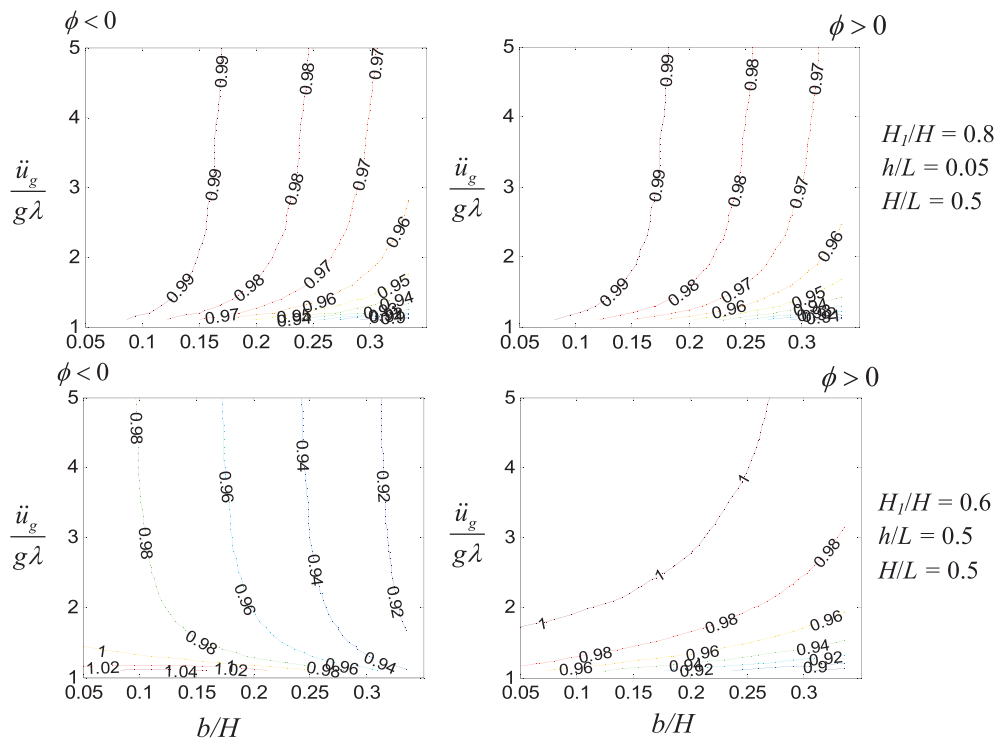


Figure 7. Evaluation of the equivalent block approximation of the asymmetric frame: overturning time error $(t_{over,blocked}/t_{over,frame})$ using κ_1 .

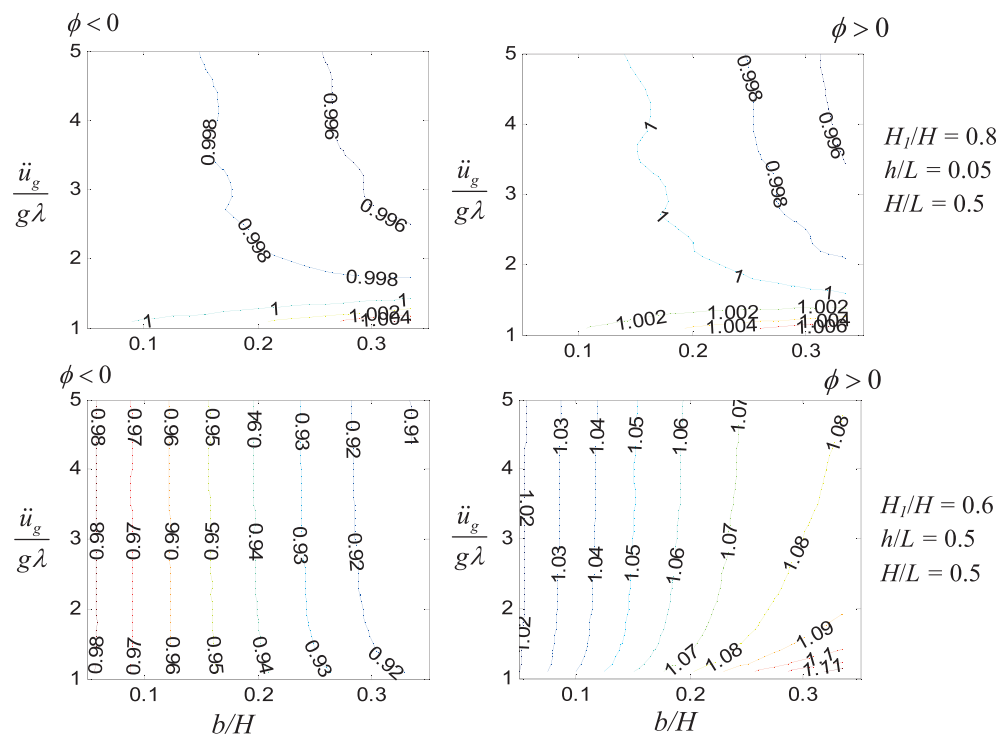


Figure 8. Evaluation of the equivalent block approximation of the asymmetric frame: overturning time error $(t_{over,blocked}/t_{over,frame})$ using κ_2 .

5.2.1. Equation of motion and problem formulation. Unlike the asymmetric frame, the arch is comprised of numerous blocks, so the hinge locations of the three-block mechanism are not immediately obvious, and could change throughout the motion. As in previous studies [40, 41], it is assumed that the hinge locations are those of the quasi-static collapse mechanism, and that the locations of the hinges are assumed fixed once rocking commences. Computational [41] and experimental [42] results indicate that these assumptions are reasonable and effective. Regardless, the accuracy of this simplification is extraneous to the current study, which takes the assumed mechanism as the starting point to investigate dynamic equivalence.

The geometry of the arch is defined by the inclusion angle β , thickness t_a , centerline radius r_a , and number of blocks n . To remove the effect of the number of blocks, a very large number of blocks were specified, allowing hinges to form essentially anywhere, and resulting in a minimum uplift parameter (λ) and the corresponding mechanism.

The kinematics of the rocking arch are similar to the asymmetric frame, and the equation of motion is therefore also described by Eqs. (8) and (32), if the pertinent arch parameters are substituted for their asymmetric frame counterparts. Similarly, the critical rotation angle (ϕ_{cr}) and the uplift parameter (λ) can be found using Eqs. (9) and (10), respectively. For the arch, the hinge locations are dependent on the geometry (t_a, r_a, β) and are determined numerically, and Eqs. (8) and (9) are solved numerically as well.

Likewise, the linearized equation of motion about the point of unstable equilibrium is again described by Eq. (12), where

$$\begin{aligned}
 I_{eq} &= \left\{ \begin{aligned} &I_{AB} + I_{CD}f_{CD}(\phi_{cr})^2 + I_{BC}f_{BC}(\phi_{cr})^2 + \\ &m_{BC}|AB| \left[|AB| + 2\bar{r}_{BC} \cos(\phi_{cr} - \phi_{BC}(\phi_{cr}) - \psi_{BC})f_{BC}(\phi_{cr}) \right] \end{aligned} \right\} \\
 G_{eq} &= - \left\{ \begin{aligned} &m_{BC}\bar{r}_{BC} \begin{bmatrix} \cos(\phi_{BC}(\phi_{cr}) + \psi_{BC})f'_{BC}(\phi_{cr}) \\ -m_{BC}\bar{r}_{BC} \sin(\phi_{BC}(\phi_{cr}) + \psi_{BC})f_{BC}(\phi_{cr})^2 \end{bmatrix} \\ &+ m_{CD}\bar{r}_{CD} \begin{bmatrix} \cos(\phi_{CD}(\phi_{cr}) + \psi_{CD})f'_{CD}(\phi_{cr}) - \sin(\phi_{CD}(\phi_{cr}) + \psi_{CD})f_{CD}(\phi_{cr})^2 \\ -m_{AB}\bar{r}_{AB} \sin(\phi_{cr} + \psi_{AB}) - m_{BC}AB \sin\phi_{cr} \end{bmatrix} \end{aligned} \right\} \quad (39) \\
 B_{eq} &= \left\{ \begin{aligned} &m_{AB}r_{AB} \sin(\phi_{cr} + \psi_{AB}) + m_{CD}r_{CD} \sin[\phi_{CD}(\phi_{cr}) + \psi_{CD}]f_{CD}(\phi_{cr}) \\ &+ m_{BC}r_{BC} \sin[\phi_{BC}(\phi_{cr}) + \psi_{BC}]f_{BC}(\phi_{cr}) + m_{BC}AB \sin\phi_{cr} \end{aligned} \right\}
 \end{aligned}$$

The only difference between Eqs. (38) and (39) is that $|AB| = 2R_0$, and that ψ_{AB} and ψ_{CD} are zero for the asymmetric frame, while they are nonzero for the arch. Note that r_{AB} , r_{BC} , and r_{CD} are the distance between the hinge and center of mass of the relevant arch segment (Figure 9) and are the equivalent of R_0 , r_{BC} , and R_l for the asymmetric frame.

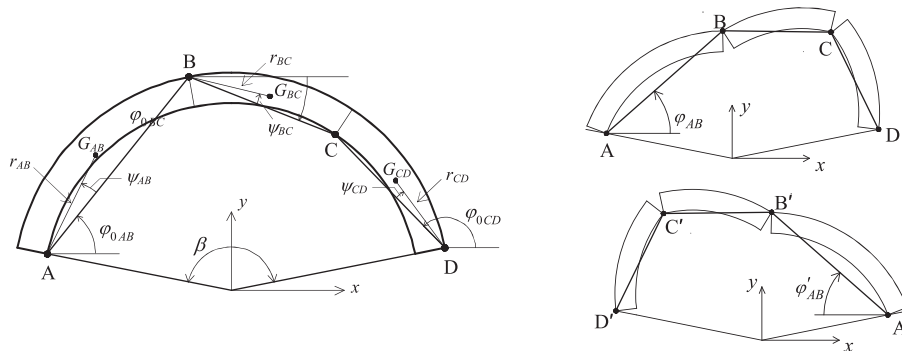


Figure 9. Geometry and symmetric rocking mechanisms of the arch.

5.2.2. *Linearization results.* The critical rocking parameters are plotted in Figure 10 for a range of practical arch geometries. Note that p is affected by the overall scale of the structure, and is therefore presented in dimensionless form, while ϕ_{cr} and λ are already dimensionless. As expected, increasing the inclusion angle (β) or decreasing the thickness both increase the effective slenderness of the arch, causing a decrease in ϕ_{cr} and λ . Further, both of these parameters have a smaller effect on p , indicating a relatively smaller change in the effective scale of the arch. Figure 10 (bottom right) also presents the error associated with the uplift acceleration caused by the linearized formulation. Because of the arch geometry and kinematics, the linearization process causes a larger error in the prediction of uplift acceleration than for the previous structures considered.

Figures 11–13 present the error associated with the proposed methodology similarly to previous sections. In particular, Figure 11 presents the error associated with the approximation of p alone (independent of κ), as a function of the inclusion angle relative thickness of the arch. Generally, errors in free rocking period are relatively small, although they increase for less slender arches (Figure 11, bottom right). Figures 12 and 13 estimate the error associated with κ_1 and κ_2 , respectively, again considering the time required for the arch to reach the point of overturning ($t_{over,arch}$) under a constant horizontal ground acceleration. In general, the errors in overturning time in Figure 12 are relatively large compared to the equivalent results for previous structures. This is partially explained by the relatively poor approximation of uplift provided by λ_{lin} for the arch, as shown in Figure 12, particularly for lower magnitudes of ground acceleration. Use of κ_2 causes a remarkable improvement, reducing the error considerably (Figure 13).

6. ILLUSTRATIVE EXAMPLES

The preceding sections have presented a simplified approach to predict the approximate response of complicated rocking mechanisms. The viability of the approach is dependent on acceptable error. In earthquake engineering, the errors quantified in the previous sections may be acceptable, as larger uncertainties in ground motion prediction capabilities may exist. This section briefly exemplifies the utility of the described approach in this context.

6.1. Seismic response

Consider first an arbitrary asymmetric frame subjected to the horizontal ground acceleration time history in Figure 14 (top), which was recorded at Rinaldi station during the 1994 Northridge

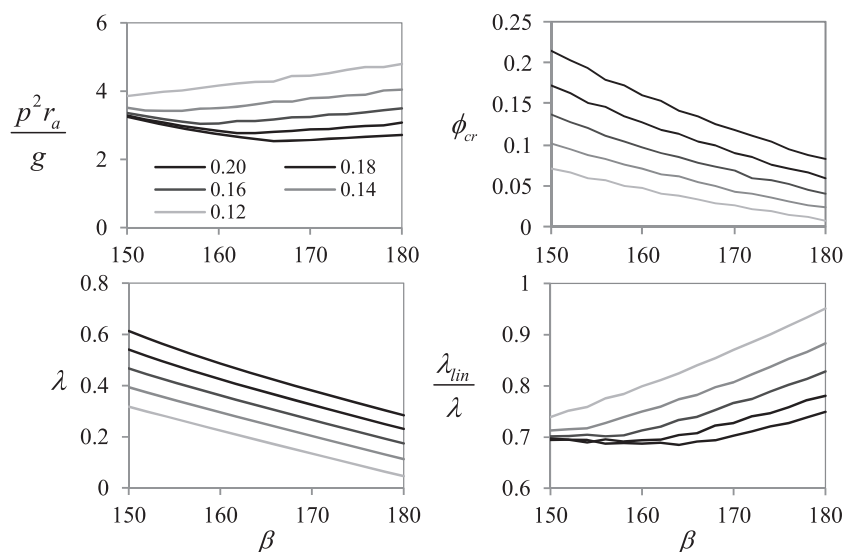


Figure 10. Essential arch rocking parameters for a range of geometries: $t_d/r_d = 0.12$ – 0.20 .

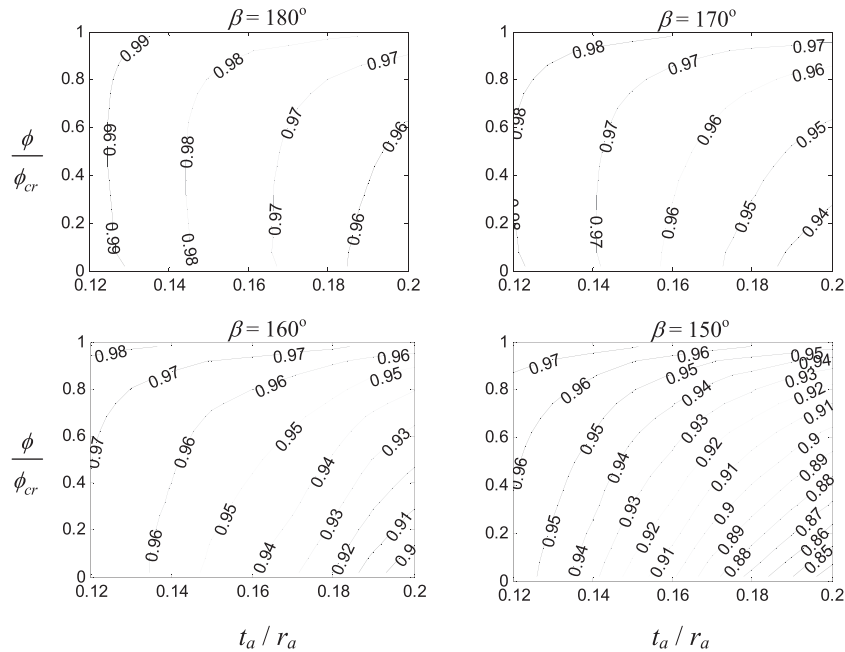


Figure 11. Linearization free rocking period error ($T_{r,blockeq}/T_{r,arch}$) associated with the equivalent block approximation of the masonry arch.

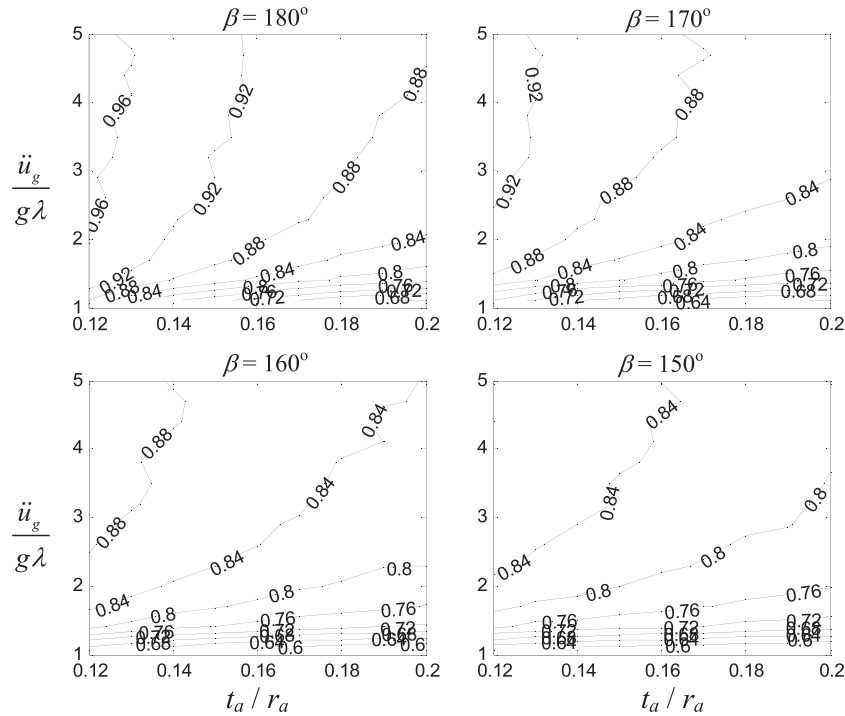


Figure 12. Overturning time error ($t_{over,blockeq}/t_{over,arch}$) associated with the equivalent block approximation of the masonry arch when using κ_1 .

earthquake [43]. The response of the asymmetric frame to the entire earthquake record, using both the nonlinear and linear formulations in Section 5.1, is shown in Figure 14.

Note that this frame is highly asymmetric, with $\lambda_n=0.241$ and $\lambda_p=0.197$, where the subscripts denote the two rocking directions. The response compares relatively well, indicating the advantage

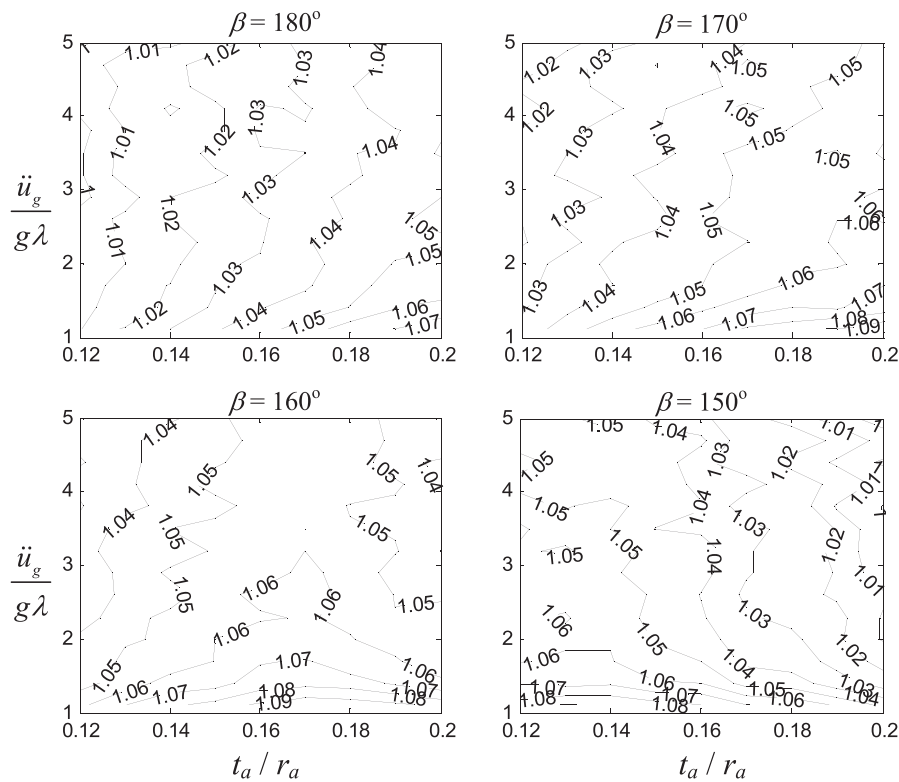


Figure 13. Overturning time error ($t_{over,blockeq}/t_{over,arch}$) associated with the equivalent block approximation of the masonry arch when using κ_2 .

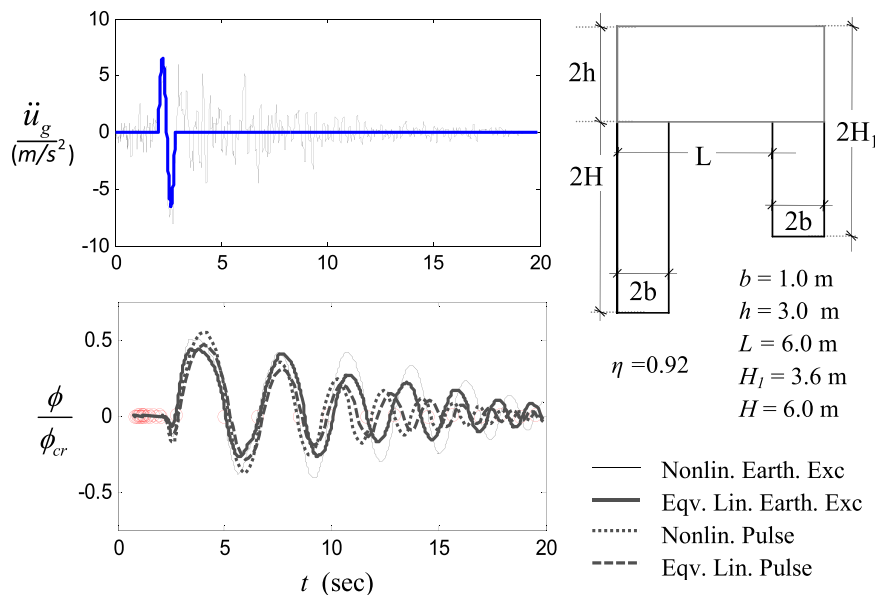


Figure 14. Seismic response of an asymmetric rocking frame: Northridge-Rinaldi earthquake ground motion and frame geometry (top), rocking response (bottom).

of the linearized approach. In this case, the earthquake contains a primary acceleration impulse, highlighted as a single period sine pulse. The response of the frame to this sine pulse alone is also plotted in Figure 14 bottom, and the dominance of the pulse is evident.

6.2. Response to pulse-type excitations

Several studies have considered the rocking response to pulses described as simple trigonometric functions (e.g. [15, 16]) and have demonstrated why rocking structures are particularly vulnerable to pulse-type earthquakes. The equivalences derived in the preceding sections, combined with the use of dimensionless variables, are particularly advantageous for this type of loading. In light of the derivations herein, the dimensionless groups defined in [16] can be slightly modified, yielding

$$\frac{\phi}{\phi_{cr}} = f\left(\frac{\omega_g}{p}, \frac{a_g}{g\lambda}, pt, \eta\right) = f(\omega, a, \tau, \eta) \tag{40}$$

where a_g and ω_g are the amplitude and circular frequency of the acceleration pulse, respectively, and θ_{cr} and λ have replaced α in the similar equation in [16]. The use of either λ_{lin} or λ in Eq. (40) corresponds to a scaling parameter of κ_1 or κ_2 , respectively.

Using the dimensionless groups in equation Eq. (40), the maximum response to a sinusoidal impulse can be directly calculated [16]:

$$\frac{\phi_{max}}{\phi_{cr}} = 1 - \sqrt{1 - \eta^2(1 - D_0^*)} \tag{41}$$

where:

$$D_0^* = \left(\frac{\omega}{\omega^2 + 1}\right)^2 \left\{ \omega^2 - 2a^2 + 1 + (\sqrt{a^2 - 1} + \omega)ae^{-(2\pi - \sin^{-1}(1/a))/\omega} + (\sqrt{a^2 - 1} - \omega)ae^{(2\pi - \sin^{-1}(1/a))/\omega} \right\} \tag{42}$$

Thus, Eqs. (41) and (42) can be used to directly approximate the maximum response of any structure with equivalence to the symmetric block. For some geometries, these equations are less accurate, and response spectra plots can instead be employed. A similar approach is possible for the asymmetric frame, although alternate equations and spectra, derived using asymmetric blocks, would be required.

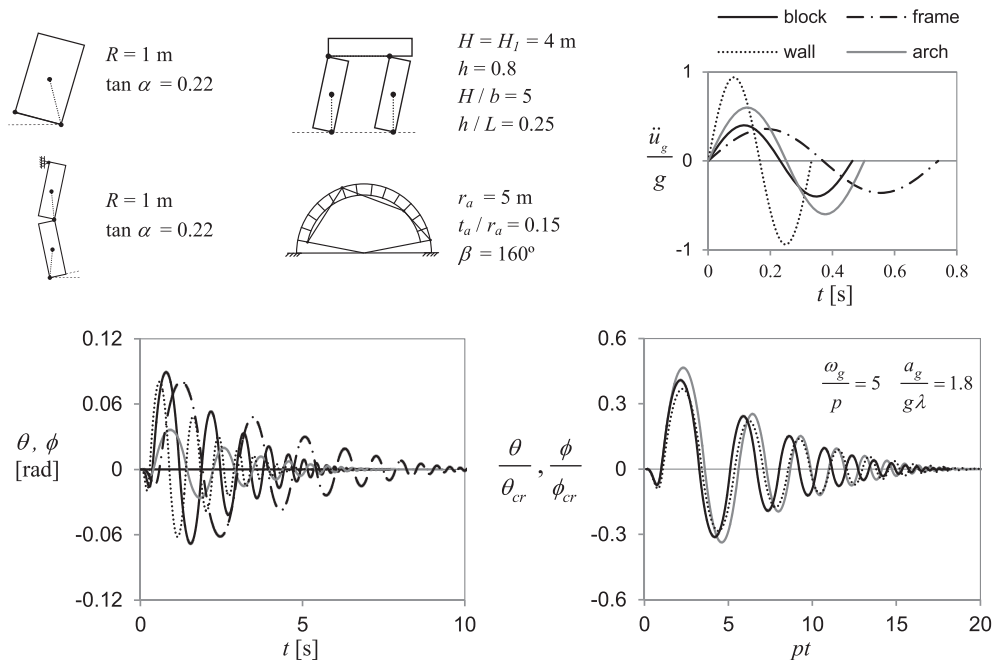


Figure 15. Comparison of pulse-type ground motions to which different structures are equivalently vulnerable. Responses are calculated using the relevant nonlinear equations of motion.

Alternatively, the response of frames with relatively small asymmetry could be approximated by averaging the rocking parameters in the two directions.

The dimensionless groups mentioned earlier are also useful to characterize the relative vulnerability of a variety of completely different structures to pulse-type ground motions. For example, consider the four structures shown in Figure 15. When subjected to the corresponding impulses shown, these structures have very different dimensional responses, but very similar nonlinear dimensionless responses (identical for the block and symmetric frame), and identical linearized dimensionless responses (not shown). Thus, these structures are (approximately) equivalently vulnerable to the impulses shown.

7. CONCLUSIONS

This study considers approximate equivalence between three types of SDOF rocking structures, which are extremely common mechanical systems: single block mechanisms (Section 2), two-block mechanisms (Section 4), and three-block mechanisms (Section 5). Importantly, this equivalence is considered for structures which can only sustain relatively small rotations before instability and therefore collapse.

The proposed methodology, which hinges on local linearization of nonlinear equation of motion, effectively yields the essential rocking parameters required to derive approximate equivalence with the rocking block. The error associated with linearization has been quantified and is affected by both the geometry and the kinematics of the mechanism. For cases where larger linearization errors occur, an alternate linearization approximation, which preserves the actual uplift acceleration of the nonlinear system, is proposed. For the masonry arch, this alternate procedure effectively reduces the error.

The level of acceptable error is application dependent. However, for many applications in the field of earthquake engineering, the order of magnitude of the errors found herein may be acceptable in comparison to relatively large uncertainties associated with ground motion prediction.

ACKNOWLEDGEMENTS

Financial support was provided by the Engineering and Physical Sciences Research Council of the United Kingdom, under grant reference number EP/H032657/1, and the Research Grants Council of Hong Kong, under grant reference number ECS 639613. Discussions with Professor Chris Calladine of the University of Cambridge are also gratefully acknowledged.

REFERENCES

1. Milne J. Experiments in observational seismology. *Journal of the Seismological Society of Japan* 1881; **3**:12–64.
2. Housner GW. The behavior of inverted pendulum structures during earthquakes. *Bulletin of the Seismological Society of America* 1963; **53**(2):403–417.
3. Spanos PD, Koh A. Rocking of rigid blocks due to harmonic shaking. *Journal of Engineering Mechanics (ASCE)* 1984; **110**(11):1627–1642. DOI: 10.1061/(ASCE)0733-9399(1984)110:11(1627).
4. Hogan SJ. On the dynamics of rigid-block motion under harmonic forcing. *Proceedings of the Royal Society A* 1989; **425**:441–476. DOI: 10.1098/rspa.1989.0114.
5. Hogan SJ. The many steady state responses of a rigid block under harmonic forcing. *Earthquake Engineering and Structural Dynamics* 1990; **19**:1057–1071. DOI: 10.1002/eqe.4290190709.
6. Lenci S, Rega G. A dynamical systems approach to the overturning of rocking blocks. *Chaos, Solitons & Fractals* 2006; **28**:527–542. DOI: 10.1016/j.chaos.2005.07.007.
7. Augusti G, Sinopoli A. Modelling the dynamics of large block structures. *Meccanica* 1992; **27**(3):195–211. DOI: 10.1007/BF00430045.
8. Lipscombe PR, Pellegrino S. Free rocking of prismatic blocks. *Journal of Engineering Mechanics (ASCE)* 1993; **119**(7):1387–1410. DOI: 10.1061/(ASCE)0733-9399(1993)119:7(1387).
9. Allen R, Oppenheim I, Parker A, Bielak J. On the dynamic response of rigid body assemblies. *Earthquake Engineering and Structural Dynamics* 1986; **14**(6):861–876. DOI: 10.1002/eqe.4290140604.
10. Sinopoli A, Sepe V. Coupled motion in the dynamic analysis of a three block structure. *Applied Mechanics Reviews* 1993; **46**(11S):S185–S197. DOI: 10.1115/1.3122636.
11. Andreus U, Casini P. Dynamics of three-block assemblies with unilateral deformable contacts. Part 2: actual application. *Earthquake Engineering and Structural Dynamics* 1999; **28**(12):1637–1649.
12. Spanos PD, Roussis PC, Politis NPA. Dynamic analysis of stacked rigid blocks. *Soil Dynamics and Earthquake Engineering* 2001; **21**(7):559–578. DOI: 10.1016/S0267-7261(01)00038-0.

13. Yim C, Chopra AK, Penzien J. Rocking response of rigid blocks to earthquakes. *Earthquake Engineering and Structural Dynamics* 1980; **8**(6):565–587. DOI: 10.1002/eqe.4290080606.
14. DeJong MJ. Amplification of rocking due to horizontal ground motion. *Earthquake Spectra* 2012; **28**(4):1405–1421. DOI: 10.1193/1.4000085.
15. Zhang J, Makris N. Rocking response of free-standing blocks under cycloidal pulses. *Journal of Engineering Mechanics (ASCE)* 2001; **127**(5):473–483. DOI: 10.1061/(ASCE)0733-9399(2001)127:5(473).
16. Dimitrakopoulos EG, DeJong MJ. Revisiting the rocking block: closed-form solutions and similarity laws. *Proceedings of the Royal Society A* 2012; **468**(2144):2294–2318. DOI: 10.1098/rspa.2012.0026.
17. Voyagaki E, Psycharis IN, Mylonakis G. Rocking response and overturning criteria for free standing rigid blocks to single-lobe pulses. *Soil Dynamics and Earthquake Engineering* 2013; **46**:85–95.
18. Beck JL, Skinner RI. The seismic response of a reinforced concrete bridge pier designed to step. *Earthquake Engineering and Structural Dynamics* 1974; **2**(4):343–358. DOI: 10.1002/eqe.4290020405.
19. Kelly JM, Tszto DF. Earthquake simulation testing of a stepping frame with energy-absorbing devices. *Bulletin of the New Zealand National Society for Earthquake Engineering* 1977; **10**(4):196–207.
20. Deierlein G, Krawinkler H, Ma X, Eatherton M, Hajjar J, Takeuchi T, Kasai K, Midorikawa M. Earthquake resilient steel braced frames with controlled rocking and energy dissipating fuses. *Steel Construction* 2011; **4**(3):171–175. DOI: 10.1002/stco.201110023.
21. Espinoza AO. Seismic performance of reinforced concrete bridges allowed to uplift during multi-directional excitation. Ph.D. Dissertation; University of California, Berkeley, 2011.
22. Pampanin S. Reality-check and renewed challenges in earthquake engineering: implementing low-damage structural systems – from theory to practice, *Proceedings of the 15th World Conference on Earthquake Engineering*. Lisbon, Portugal, 2012.
23. Dimitrakopoulos EG, DeJong MJ. Overturning of retrofitted rocking structures under pulse-type excitations. *Journal of Engineering Mechanics (ASCE)* 2012; **138**(8):963–972. DOI: 10.1061/(ASCE)JEM.1943-7889.0000410.
24. ASCE/SEI Standard 43-05. Seismic design criteria for structures, systems, and components in nuclear facilities, American Society of Civil Engineers and Structural Engineering Institute, 2005.
25. Makris N, Konstantinidis D. The rocking spectrum and the limitation of practical design methodologies. *Earthquake Engineering and Structural Dynamics* 2003; **32**(2):265–289. DOI: 10.1002/eqe.223
26. Prieto F, Lourenço PB, Oliveira CS. Impulsive Dirac-delta forces in the rocking motion. *Earthquake Engineering and Structural Dynamics* 2004; **33**(7):839–857. DOI:10.1002/eqe.381.
27. ElGawady MA, Ma Q, Butterworth JW, Ingham J. Effects of interface material on the performance of free rocking blocks. *Earthquake Engineering and Structural Dynamics* 2010; **40**:375–392. DOI: 10.1002/eqe.1025.
28. Palmeri A, Makris N. Linearization and first-order expansion in non-linear dynamics: a case study. *Earthquake Engineering and Structural Dynamics* 2008; **37**(7):1065–108. DOI: 10.1002/eqe.799.
29. Allen RH, Duan X. Effects of linearizing on rocking-block toppling. *Journal of Structural Engineering, ASCE* 1995; **121**:1146–1149. DOI: 10.1061/(ASCE)0733-9445(1995)121:7(1146).
30. DeJong MJ. Seismic response of stone masonry spires: analytical modeling. *Engineering Structures* 2012; **40**:556–565. DOI: 10.1016/j.engstruct.2012.03.010.
31. DeJong MJ, Vibert C. Seismic response of stone masonry spires: computational and experimental modeling. *Engineering Structures* 2012; **40**(4):566–574. DOI: 10.1016/j.engstruct.2012.03.001.
32. Makris N, Vassiliou MF. Planar rocking response and stability analysis of an array of free-standing columns capped with a freely supported rigid beam. *Earthquake Engineering and Structural Dynamics* 2013; **42**(3):431–449. DOI: 10.1002/eqe.2222.
33. Meirovitch L. *Elements of Vibration Analysis* (2nd edn). McGraw-Hill: Boston, Massachusetts, 1986.
34. Doherty K, Griffith MC, Lam N, Wilson J. Displacement-based seismic analysis for out-of-plane bending of unreinforced masonry walls. *Earthquake Engineering and Structural Dynamics* 2002; **31**(4):833–850. DOI: 10.1002/eqe.126.
35. Ciancio D, Augarde C. Capacity of unreinforced rammed earth walls subject to lateral wind force: elastic analysis versus ultimate strength analysis. *Materials and Structures* 2013; **46**(9):1569–1585. DOI: 10.1617/s11527-012-9998-8.
36. Sorrentino L, Masiani R, Griffith MC. The vertical spanning strip wall as a coupled rocking rigid body assembly. *Structural Engineering and Mechanics* 2008; **29**(4):433–453.
37. Plaut RH, Fielder WT, Virgin LN. Fractal behavior of an asymmetric rigid block overturning due to harmonic motion of a tilted foundation. *Chaos, Solitons & Fractals* 1996; **7**(2):177–196. DOI: 10.1016/0960-0779(95)00059-3.
38. Shao Y, Tung CC. Seismic response of unanchored bodies. *Earthquake Spectra* 1999; **15**(3):523–536. DOI: 10.1193/1.1586056.
39. Di Egidio A, Contento A. Investigations into the benefits of base isolation for non-symmetric rigid blocks. *Earthquake Engineering and Structural Dynamics* 2009; **38**(7):849–866. DOI: 10.1002/eqe.870.
40. Oppenheim IJ. The masonry arch as a four-link mechanism under base motion. *Earthquake Engineering and Structural Dynamics* 1992; **21**(11):1005–1017. DOI: 10.1002/eqe.4290211105.
41. De Lorenzis L, DeJong MJ, Ochsendorf J. Failure of masonry arches under impulse base motion. *Earthquake Engineering and Structural Dynamics* 2007; **36**(14):2119–2136. DOI: 10.1002/eqe.719.
42. DeJong MJ, De Lorenzis L, Adams S, Ochsendorf J. Rocking stability of masonry arches in seismic regions. *Earthquake Spectra* 2008; **24**(4):847–865. DOI 10.1193/1.2985763.
43. Chiou B, Darragh R, Gregor N, Silva W. NGA project strong-motion database. *Earthquake Spectra* 2008; **24**(1):23–44. DOI: 10.1193/1.2894831.